How to cite: *Angew. Chem. Int. Ed.* **2025**, e202511093
doi.org/10.1002/anie.202511093

Nanotubes

Exciton Trapping at Shape-Persistent Molecular Nanotubes

Victor M. Espinoza Castro[+], *Saber Mirzaei*[+], *Mohammad Bilal, Gabriella N. Ruiz, Michael J. Rose, Xu Wang, and Raúl Hernández Sánchez**

Abstract: We report a series of shape-persistent molecular nanotubes with top rim connectivity traversing from an all-*meta*- (**m**$_4$) to an all-*para*-phenylene (**p**$_4$) bridged species, including all possible members in between them. Single-crystal X-ray diffraction (SCXRD) and microcrystal electron diffraction (MicroED) data show a large torsional angle for *meta*-phenylenes relative to *para*-phenylene rings. Density functional theory (DFT) calculations reproduce the experimental torsional angles and also establish a correlation indicating a gradual increase in strain energy from **m**$_4$ (~31 kcal mol^{-1}) to **p**$_4$ (~90 kcal mol^{-1}). Structural transitions from **m**$_4$ to **p**$_4$ lead to additional correlations such as a shift in the lowest absorption wavelength from 330 to 394 nm, a sizeable red shift in the maximum emission wavelength from 444 to 546 nm, and a decrease in fluorescence quantum yield from 0.76 to 0.20, respectively. Time-dependent (TD)-DFT analysis of the relaxed excited state ($S_{1'}$) geometry shows a progression of exciton delocalization as *para*-phenylenes are introduced into **m**$_4$ en route to **p**$_4$, while the overall molecular size remains constant. This effect is directly related to increased π-conjugation within the nanotube's top-segment and demonstrates how exciton trapping can take place without changing the nanotube's physical size, e.g., diameter and length.

Aromaticity is a central concept in science that describes a class of highly stable cyclic molecules, in which the electrons are delocalized through conjugated π orbitals.[1] In Hückel and Clar-obeying systems, aromatic molecules are typically planar for optimal orbital overlap.[2,3] Synthetic strategies to deviate aromatic frameworks away from planarity have fascinated scientists for almost a century,[4–10] becoming a standalone research field over the last three decades.[11–14] These contorted aromatic systems exhibit novel properties, such as singlet fission behavior,[15–17] record-breaking chirality in helicenes,[18–20] develop into molecular Möbius topologies,[21–26] serve as curved hosts for supramolecular chemistry,[27–34] function as bioimaging agents,[35,36] and expand the toolbox of electronic materials for organic devices.[37–42] Radially π-conjugated compounds fall under the umbrella of contorted aromatics and were first established in the late 90's.[8,43] Later, seminal synthetic developments[44–46] between 2008 and the 2010's created a toolbox that led to a vast number of applications.[47–51] Currently, synthetic strategies to build contorted radial aromatic systems, specifically [*n*]cyclo-*para*-phenylenes ([*n*]CPPs), are commonplace in the literature.[52–57] Novel phenomena have been reported within the family of [*n*]CPPs. Notably, they display a bathochromic fluorescence shift and vanishing quantum yields (ϕ_f) as the ring decreases in size,[52,58] accompanied by a decrease in the HOMO-LUMO gap.[59] These properties follow the same trend even when the symmetry of [*n*]CPPs is decreased to *m*[*n*]CPPs (Figure 1a). In contrast, linear oligophenylenes display the opposite behavior.[60,61]

Several interconnected factors contribute to the photophysical properties of [*n*]CPPs. In principle, increasing the number of *para*-phenylenes in [*n*]CPPs leads to greater surface for exciton delocalization. However, this increased size also reduces strain energy between the phenylene units and facilitates exciton self-trapping within a section of the [*n*]CPP.[62] It is, therefore, challenging to decouple the variables affecting exciton confinement in nanohoops as these also change when varying the ring size.[63,64] Herein, we report a class of six nanotubes relatively maintaining their overall molecular size throughout (Figure 1b), where their top-rim connectivity dictates the extent of exciton confinement therefore tuning their fluorescence emission approximately from blue to yellow. In analogy to quantum dots (QDs), while the size of the dot dictates the size of the box (Figure 1a), in the classic particle-in-a-box model;[65–67] here, the nanotube top-rim bond connectivity and changing π-conjugation dictates the box size without changing the physical size of the nanotube.

[*] V. M. Espinoza Castro[+], S. Mirzaei[+], M. Bilal, R. Hernández Sánchez
Department of Chemistry, Rice University, 6100 Main St., Houston, Texas 77005, USA
E-mail: raulhs@rice.edu

S. Mirzaei[+], R. Hernández Sánchez
Department of Chemistry, University of Pittsburgh, 219 Parkman Ave., Pittsburgh, Pennsylvania 15260, USA

G. N. Ruiz, M. J. Rose
Department of Chemistry, University of Texas at Austin, 100 East 24th St., Austin, Texas 78712, USA

X. Wang
Shared Equipment Authority, Rice University, 6100 Main St., Houston, Texas 77005, USA

R. Hernández Sánchez
Rice Advanced Materials Institute, Rice Sustainability Institute, Rice WaTER Institute, Rice University, Houston, Texas 77005, USA

[+] Both authors contributed equally to this work.

Additional supporting information can be found online in the Supporting Information section

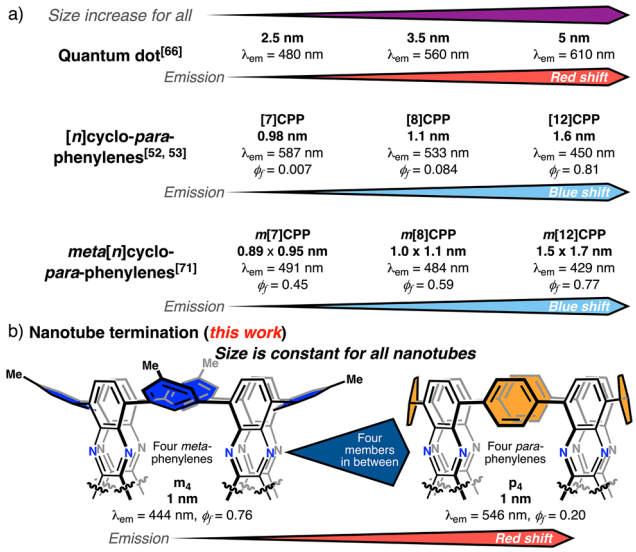

Figure 1. Structure-electronic structure relationships of a) inorganic and organic species compared to b) the molecular nanotubes reported herein.

Our research group recently reported tubularene **p**$_4$,[68] which is synthesized from **1** in one step via an eight-fold Suzuki–Miyaura cross-coupling reaction with 1,4-phenylenediboronic acid bis(pinacol) ester (Scheme 1). A slight change of the connecting *para*-phenylene to 5-methyl-1,3-phenylenediboronic acid bis(pinacol) ester results in **m**$_4$ with 2.9% isolated yield (for simplicity the 5-methyl-1,3-phenylene unit is referred to as 1,3-phenylene throughout this manuscript).[69] Carrying out the cross-coupling reaction with a 1:1 mixture of both bis(pinacol) esters, 1,4-phenylenediboronic acid and 5-methyl-1,3-phenylenediboronic acid, results in a complex mixture of all possible members ranging from the all-*meta*- (**m**$_4$) to the all-*para*-phenylene (**p**$_4$) nanotubes. Isolation of all members in the series: **m**$_4$, **m**$_3$**p**$_1$, ***anti*-m**$_2$**p**$_2$, ***syn*-m**$_2$**p**$_2$, **m**$_1$**p**$_3$, to **p**$_4$, was achieved through a combination of standard column chromatography, preparatory thin layer chromatography, and high-performance liquid chromatography as described in the Supplementary Information. As noted in Scheme 1, isolated yields range from as low as 0.08% for **p**$_4$ to as high as 1.0% for **m**$_3$**p**$_1$.

All species in the series from **m**$_4$ to **p**$_4$ are rigid. A large rotational barrier of around 30 kcal mol^{-1} was computed for the bridging *para*-phenylene in **p**$_4$,[68] which we expect to be similar in magnitude for species containing one to three *para*-phenylenes. The 1,3-phenylenes are not expected to rotate as their connectivity already diminishes strain in the nanotube. In solution, **m**$_4$ displays an ideal C_{4v} symmetry with five unique aromatic resonances in its ^{1}H NMR spectrum (Figure S1), akin to **p**$_4$. The species **m**$_3$**p**$_1$, ***syn*-m**$_2$**p**$_2$, and **m**$_1$**p**$_3$ share an ideal C_s point group symmetry having 17 (Figures S6), 15 (Figures S16), and 18 (Figures S21) unique aromatic resonances, respectively (see Supporting Information). Moreover, the ideal C_2 rotation axis in ***anti*-m**$_2$**p**$_2$ raises its symmetry producing a fewer number of unique proton environments collapsing the total number of aromatic resonances to 10 (Figure S11). Resonance "*a*" is particularly important as it serves as a direct reporter of the overall molecular symmetry with chemical shift (δ) positions at 5.96 in **m**$_4$; a^1 = 6.11, a^2 = 5.62 in **m**$_3$**p**$_1$; 5.33 in ***anti*-m**$_2$**p**$_2$; 5.78 in ***syn*-m**$_2$**p**$_2$; and 5.57 ppm in **m**$_1$**p**$_3$. The small variation of δ for "*a*" between 5.33 and 5.96 ppm suggest its relatively similar environment across all nanotubes in the series. The general upfield shift across this series indicates a strong shielding effect coming from the inner section of the tube. A similar phenomenon is observed in *m*[*n*]CPPs,[70] for instance, the series reported by Jasti et al. for n = 5–8, 10, and 12, displays resonance "*a*" in their systems shifting upfield from 7.12 in *m*[12]CPP to 4.80 ppm in *m*[5]CPP as a result of the nanohoop rigidification (Figure S26).[71] The same trend is observed in cyano-*m*[*n*]CPPs, where resonance "*a*" shifts upfield from 7.07 in cyano-*m*[10]CPP to 6.04 ppm in cyano-*m*[6]CPP.[72] Hence, changing the number of *para*-phenylenes (n) in these series, *m*[*n*]CPPs and cyano-*m*[*n*]CPPs, cannot inherently disentangle the effect of ring size and torsional angles that lead to exciton trapping.

All species in the series from **m**$_4$ to **p**$_4$ display quadrupole time-of-flight mass spectrometry (qToF MS) patterns matching their corresponding simulated isotopic distributions (Figure 2a–e). Gratifyingly, high-quality crystals of **m**$_4$, **m**$_3$**p**$_1$, and ***anti*-m**$_2$**p**$_2$ allowed us to determine their molecular structure via single-crystal X-ray diffraction (SCXRD, Figure 2f–h). Crystals of ***syn*-m**$_2$**p**$_2$ were too small preventing their structure determination via SCXRD; however, they were suitable for microcrystal electron diffraction (MicroED, Figure 2i).[73] Last, all attempts to determine the structure of **m**$_1$**p**$_3$ failed; hence, its structure was optimized via DFT at the B3LYP-D3(BJ)/6–31G(d) level of theory (Figure 2j). At first glance, all structures in this series of tubularenes display the *meta*-phenylene rings played out and adopting a large torsion angle α relative to their immediate quinoxaline nanotube's walls. The angle α is larger than the torsion angle β resulting from the *para*-phenylenes and the wall (Figure 2). Overall, spectroscopic and crystallographic characterization establish all members in the series from **m**$_4$ to **p**$_4$ as rigid nanotubes.

Intrigued to understand the relationship imposed by the molecular structure on the tubularene's electronic properties, we collected UV–vis absorption and emission spectra of **m**$_4$, **m**$_3$**p**$_1$, ***anti*-** and ***syn*-m**$_2$**p**$_2$, and **m**$_1$**p**$_3$ in dichloromethane at room temperature. We also reproduced previously reported **p**$_4$ optical data for comparative purposes.[68] Following literature precedent,[74] we simulated the absorption properties of all nanotubes by conducting time-dependent (TD) DFT calculations using their optimized ground state geometry S_0 obtained at the B3LYP-D3(BJ)/6-31G(d) level of theory. First, the HOMO → LUMO transition is Laporte forbidden in higher symmetry compounds: **m**$_4$, ***anti*-m**$_2$**p**$_2$, and **p**$_4$ (Table S2). We observe a low energy absorption band in **p**$_4$ at λ_{max} = 394 nm (Figure 3a), which is described by a combination of HOMO → LUMO + 1 and HOMO - 1 → LUMO. A bathochromic shift is observed for the HOMO → LUMO + 1 absorption peak as 1,4-phenylene rings are introduced into **m**$_4$ by replacing 1,3-phenylene groups until **p**$_4$ (Figure S34). Fluorescence spectra show a similar bathochromic shift in emission maximum (λ_{em})

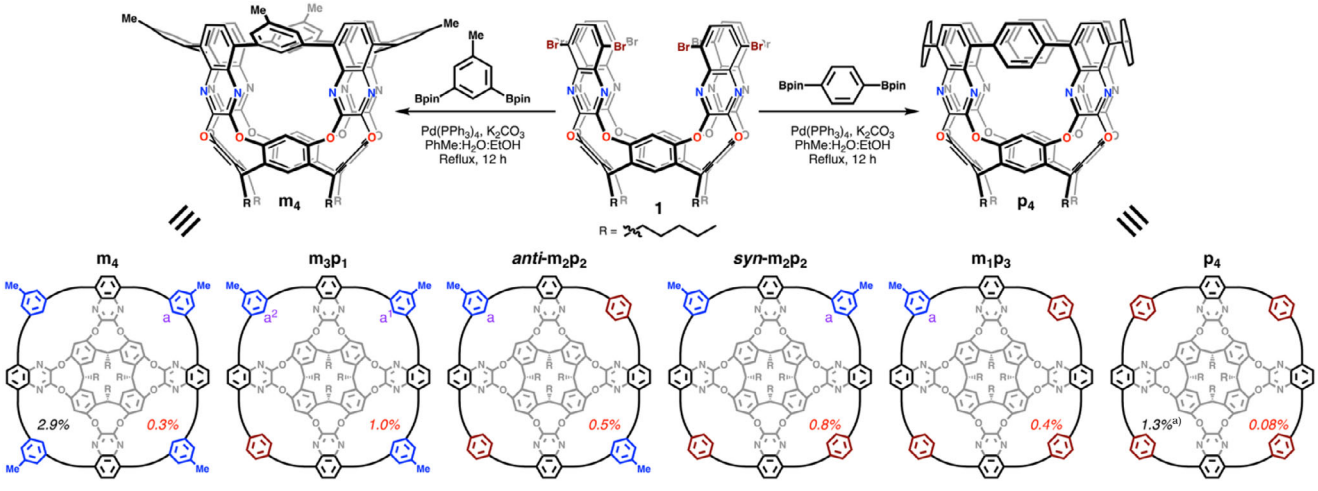

Scheme 1. Nanotube synthesis. Isolated yields in red correspond to the reaction of **1** plus a 1:1 mixture of 1,4-phenylenediboronic acid bis(pinacol) ester and 5-methyl-1,3-phenylenediboronic acid bis(pinacol) ester. Yields in black are from using a single diboronic ester. [a] Yield from Ref. [68]

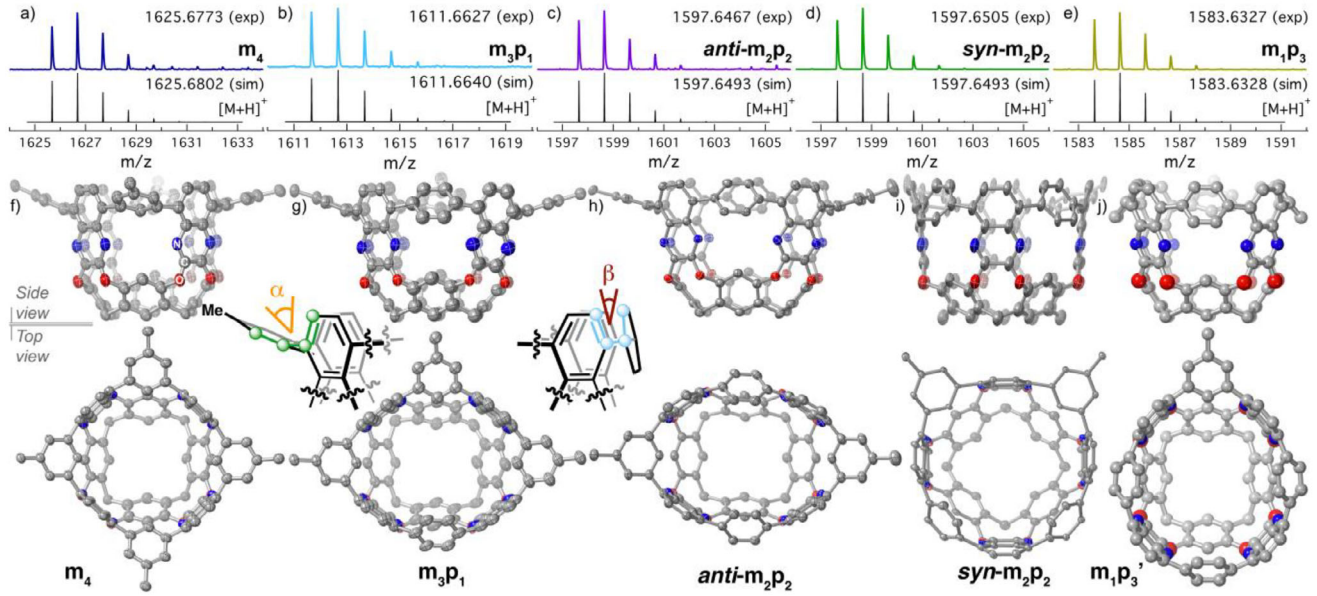

Figure 2. Characterization of molecular nanotubes **m4**, **m3p1**, ***anti*-m2p2**, ***syn*-m2p2**, and **m1p3**. a)–e) Experimental qToF MS molecular ion peaks (colored traces). Black traces correspond to the simulated $[M + H]^+$ isotopic distributions. Molecular structures of f) **m4**, g) **m3p1**, and h) ***anti*-m2p2** collected via SCXRD at 110, 140, and 100 K, respectively. i) The structure of ***syn*-m2p2** was collected via MicroED. Thermal ellipsoids of all structures are set at 50% probability level. The H atoms, R groups (*n*-pentyl), and any solvent molecules are omitted for clarity. j) Structure of **m1p3'** (R = Me) optimized via DFT at the B3LYP-D3(BJ)/6–31G(d) level of theory. Insets: Illustrations of the torsional angles α and β.

monotonically moving from **m4** at $\lambda_{em} = 444$ nm to **p4**, which emits at $\lambda_{em} = 546$ nm (Figure 3b). This trend is visualized in dilute solutions of these nanotubes, e.g., under white light they form relatively similar colorless solutions (Figure 3c); however, when these are observed under UV light (365 nm) a clear progression from blue to yellow emission is detected from **m4** to **p4** (Figure 3d), respectively. In comparison, the fluorescence maxima of [*n*]CPPs redshifts as their molecular ring size decreases. For instance, [12]CPP ($\phi_f = 0.81$), [8]CPP ($\phi_f = 0.084$), and [7]CPP ($\phi_f = 0.007$), emit at 450, 533, and 587 nm, respectively,[52,58,75] while the smaller [6]- and [5]CPP are essentially nonemissive.[76–78] Theoretical and experimental work explain this feature by determining that the lowest singlet excited state ($S_{1'}$) is no longer centrosymmetric on [*n*]CPPs containing eight or more *para*-phenylenes due to local distortion of the nanohoop that results in exciton self-trapping.[63,74,79–83] In the more rigid [6]- and [5]CPP, emissive relaxation from $S_{1'}$ to S_0 is Laporte forbidden due to the conservation of orbital centrosymmetry. Breaking the [*n*]CPP's symmetry and disrupting π-conjugation by introducing a single *meta*-phenylene ring, *m*[*n*]CPP, turns on fluorescence in the small congeners producing [ϕ_f, λ_{em} (nm)] of [0.450, 491], [0.224, 510], and [0.014, 534] in *m*[7]-, *m*[6]-, and *m*[5]CPP, respectively.[71] Similar to [*n*]CPPs, the emission

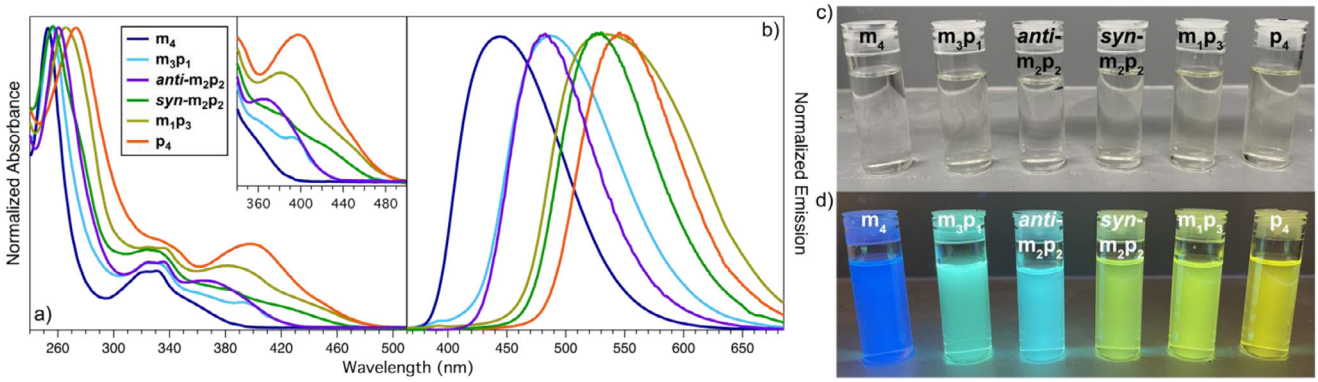

Figure 3. a) Absorption and b) emission spectra of $\mathbf{m_4}$ (navy blue), $\mathbf{m_3p_1}$ (cyan), ***anti*-$\mathbf{m_2p_2}$** (purple), ***syn*-$\mathbf{m_2p_2}$** (green), $\mathbf{m_1p_3}$ (dark yellow), and $\mathbf{p_4}$ (orange) in dichloromethane at room temperature. Emission data were collected by light excitation at 330 nm. Photographic image of dilute tubularenes dissolved in dichloromethane exposed to c) white and d) UV light (365 nm), respectively.

Table 1: Experimental and calculated metrics of tubularenes reported herein.

	$\mathbf{m_4}$	$\mathbf{m_3p_1}$	***anti*-$\mathbf{m_2p_2}$**	***syn*-$\mathbf{m_2p_2}$**	$\mathbf{m_1p_3}$	$\mathbf{p_4}$
SE (kcal mol^{-1})[a]	30.6(7)	45.1(7)	56.9(8)	60.9(7)	74.2(9)	89(1.1)[b]
HOMO (eV)[c]	−6.15	−5.80	−5.83	−5.63	−5.56	−5.42[b]
LUMO (eV)[c]	−2.15	−2.28	−2.26	−2.38	−2.41	−2.42[b]
E_g (eV)[c]	4.00	3.52	3.57	3.25	3.15	3.00[b]
ϕ_f	0.76	0.52	0.53	0.26	0.25	0.20[d]
λ_{max} (nm)[e]	ND	ND	365	ND	382	394[b]
λ_{em} (nm)	444	487	483	522	533	546[b]

[a] DFT-calculated values. Error on the average SE is determined from five DFT calculations at different levels of theory. [b] Data taken from reference.[68] [c] DFT-calculated values using B3LYP-D3(BJ)/6-31G(d) (see Supporting Information). [d] ϕ_f for $\mathbf{p_4}$ was remeasured and corrected from our previously reported value of 0.4.[84] [e] Lowest absorption band. ND = not determined (unresolved low energy absorption band).

maxima in *m*[*n*]CPPs redshifts as the molecular size of the nanohoop decreases. Herein, the overall molecular size of tubularenes in the series from $\mathbf{m_4}$ to $\mathbf{p_4}$ remains relatively constant while their quantum yields decrease monotonically from 0.76 in $\mathbf{m_4}$ to 0.20 in $\mathbf{p_4}$ (Table 1). Most importantly, the red shifting emission observed from $\mathbf{m_4}$ to $\mathbf{p_4}$ must be attributed to electronic structure changes emerging from their unique connectivity patterns.

To better understand the relevance of molecular rigidity, strain energies (SE) were determined using DFT methods employing homodesmotic reactions described in Figures S42 and S43. The average of five different functionals show a monotonic increase in SE from $\mathbf{m_4}$ at ~30 kcal mol^{-1} to $\mathbf{p_4}$ at ~90 kcal mol^{-1} (Tables 1 and S4). On average, 15 kcal mol^{-1} of strain are introduced for every *para*-phenylene ring added to $\mathbf{m_4}$, making a nearly linear correlation. Note that ***anti*-** and ***syn*-$\mathbf{m_2p_2}$** have almost the same SE. To quantify the structural deformation in these nanotubes, torsional angles α and β were defined as shown in Figure 2 (insets). The torsional angles α and β monotonically decline in the series from $\mathbf{m_4}$ to $\mathbf{p_4}$ with a concomitant increase in SE (Figure 4a). Interestingly, β remains relatively large across the series compared to similarly sized [*n*]CPPs; for instance, [8]- and [10]CPP have β angles of ~24(6) and ~27(4) degrees,[85] and their strain energies are 72.2 and 57.7 kcal mol^{-1},[86] respectively. Moreover, although a close structural resemblance exists between *m*[8]CPP and $\mathbf{m_1p_3}$, significant differences are noted when their DFT optimized structures are analyzed in detail. For example, *m*[8]CPP displays α, β, and SE of 50 degrees, 30 degrees, and 57 kcal mol^{-1},[71] respectively, while the structure of $\mathbf{m_1p_3}$ shows 64.02(5) degrees, 40.6(12) degrees, and 74.2(9) kcal mol^{-1}, respectively. Note that a direct comparison to [*n*]CPPs is challenging since the family of nanotubes reported herein has every other connecting group in the top-rim fixed to the resorcin[4]arene template. Overall, the latter comparison highlights the increased rigidity found in the nanotubes reported herein.

We attribute the emission properties of these nanotubes to be modulated by their overall structural topology. Reports by Tretiak,[74,87] Jasti,[71] Fernandez-Alberti,[88] Kanemitsu,[80,81] and Kim,[82] show that vibrational relaxation from the lowest singlet excited state S_1 to the distorted emission state $S_{1'}$ breaks [*n*]CPPs centrosymmetry for $n > 6$, allowing the occurrence of the $S_{1'} \rightarrow S_0$ emissive transition; whereas, the $S_{1'}$ states of smaller [*n*]CPPs ($n = 5, 6$) maintain full radial delocalization and centrosymmetry, leading to a Laporte-forbidden emission.[83] It is worth noting that emission typically occurs from the $S_{1'}$ state per Kasha's rule.[89] Although a recent report by Du shows that symmetry breaking within a bisnanohoop exhibits anti-Kasha emission (emission from an S_n to S_0); thus far, there is no indication that this phenomenon is present in our system.[90] Interested in the $S_{1'}$ geometries of all compounds from $\mathbf{m_4}$ to $\mathbf{p_4}$, we performed TD DFT geometry optimizations employing the

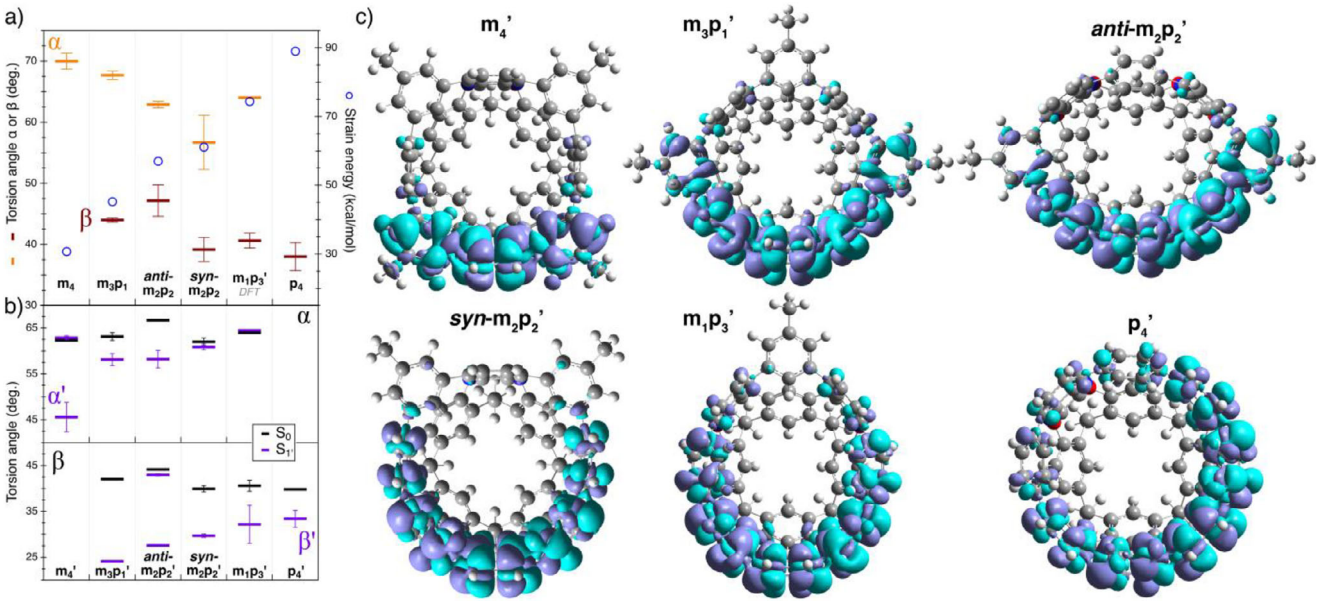

Figure 4. a) Torsion angles α and β from crystallographic data and strain energies for all nanotubes in the series $\mathbf{m_4}$, $\mathbf{m_3p_1}$, ***anti*-$\mathbf{m_2p_2}$**, ***syn*-$\mathbf{m_2p_2}$**, $\mathbf{m_1p_3}$**'**, and $\mathbf{p_4}$. b) DFT-calculated torsion angles α and β in the ground state (S_0) and TD-DFT-calculated torsion angles α' and β' for the lowest singlet excited state ($S_{1'}$). Structures were calculated at the CAM-B3LYP-D3(BJ)/6-31G(d) level of theory with dichloromethane as the solvent. c) Transition density plots at $S_{1'}$ geometries (isovalue = 0.004).

Coulomb-attenuated hybrid B3LYP (CAM-B3LYP-D3(BJ))/6-31G(d) level of theory,[91] given that long-range-corrected (LC) functionals are critical to modelling the structural distortion that follows excitonic and charged states.[74] Torsional angles α and β in S_0 and $S_{1'}$ are extracted from the DFT-optimized structures and provided in Figure 4b (full details in Table S5). The calculated ground state torsional angles reproduce β more closely than α (Figure S44). Most importantly, the excited state structures showcase a significant reduction of torsional angles α and β where exciton localization takes place. For instance, in the $S_{1'}$ state of $\mathbf{m_4}$**'** (R = Me)[92] two sets of torsional angles α' are observed, one set averaging 63 degrees, close to the value extracted from its molecular crystal structure, and one set around 46 degrees (Figure 4b). The latter one is the site of exciton localization, which is represented in the transition density plot of $\mathbf{m_4}$**'** in Figure 4c. The rest in the series containing both *meta*- and *para*-phenylenes, specifically $\mathbf{m_3p_1}$**'**, ***anti*-$\mathbf{m_2p_2}$**', ***syn*-$\mathbf{m_2p_2}$**', and $\mathbf{m_1p_3}$**'** show exciton localization exclusively across *para*-phenylenes with β' monotonically increasing from ~24 degrees in $\mathbf{m_3p_1}$**'** to ~32 degrees in $\mathbf{m_1p_3}$**'**. Note that ***anti*-$\mathbf{m_2p_2}$**' displays two significantly different β's, one at ~43 degrees essentially unperturbed relative to the ground state and a second set at ~28 degrees indicating the site of exciton localization. Last, $\mathbf{p_4}$**'** shows β' values averaging ~33 degrees, which is smaller than the calculated ground state value of β = ~40 degrees ($\beta_{experimental}$ = 38(2.4) degrees). Altogether, these torsional angle metrics inform the site of exciton localization. Furthermore, transition density plots at $S_{1'}$ geometries show the extent of exciton self-trapping across the nanotube series (Figure 4c). Qualitatively, the exciton distribution in the nanotube's aromatic topology increases from $\mathbf{m_4}$**'** to $\mathbf{p_4}$**'**. Additionally, the nanotube's quinoxaline walls increase the π-conjugated surface for the self-trapped exciton to delocalize (Figures S50–S55).[88]

Finally, shifting of the fluorescence emission in organic compounds or metal-based materials is traditionally ascribed to a change in physical size, e.g., [*n*]CPPs,[52] linear *p*-phenylenes,[93] polyaromatic hydrocarbons (PAHs),[94–96] quantum dots,[97,98] which in turn is correlated with the size of their π-conjugated surface, in the case of organic materials, or their particle size, when considering quantum dots. In this study, we show that the $\mathbf{m_4}$ to $\mathbf{p_4}$ series exhibits a red-shifting emission although the relative overall size of the nanotube is conserved. We conclude that insertion of 1,4-phenylene groups in the top rim section of the nanotube increases its π-conjugated surface, which effectively enhances delocalization of the exciton from $\mathbf{m_4}$ to $\mathbf{p_4}$. Most importantly, maintaining the overall size in this series of nanotubes, yet changing its top-rim connectivity, provides a unique opportunity to disentangle the effect of ring size and torsional angles in the study of exciton trapping.

Supporting Information

The authors have cited additional references within the Supporting Information File (Refs. [99–119]).

Acknowledgements

The authors gratefully acknowledge support from startup funding from Rice University and the University of Pittsburgh. This work was partially funded by NSF CAREER CHE-2042423. This research was funded in part by a grant

from The Welch Foundation (C-2142-20230405). M.J.R. and G.N.R. acknowledge funding from The Welch Foundation (X-F-0003-20230731) for MicroED support, as well as Welch grant F-1822. MicroED data were collected at the Sauer Structural Biology Laboratory at the University of Texas at Austin. The authors thank the support from the Center for Research Computing at Rice University and similarly the University of Pittsburgh Center for Research Computing and Data. R.H.S. would like to acknowledge the Robert A. Welch Foundation for a Young Investigator Award. S.M. acknowledges the support from the Dietrich School of Arts & Sciences Graduate Fellowship, the Andrew Mellon Predoctoral Fellowship. V.M.E.C. would like to acknowledge Hormoz Khosravi for discussions on TD DFT analysis. The authors would like to thank Dr. Christopher Pennington for his help with HRMS.

Conflict of Interests

The authors declare no conflict of interest.

Data Availability Statement

The data that support the findings of this study are available in the Supporting Information of this article.

Keywords: Exciton self-trapping · Fluorescence · Macrocycle template · Molecular nanotube · Resorcin[*n*]arenes

[1] G. Merino, M. Solà, I. Fernández, C. Foroutan-Nejad, P. Lazzeretti, G. Frenking, H. L. Anderson, D. Sundholm, F. P. Cossío, M. A. Petrukhina, J. Wu, J. I. Wu, A. Restrepo, *Chem. Sci.* **2023**, *14*, 5569–5576.
[2] T. M. Krygowski, M. K. Cyrański, *Chem. Rev.* **2001**, *101*, 1385–1420.
[3] M. Randić, *Chem. Rev.* **2003**, *103*, 3449–3606.
[4] V. C. Parekh, P. C. Guha, *J. Indian Chem. Soc.* **1934**, *11*, 95–100.
[5] W. E. Barth, R. G. Lawton, *J. Am. Chem. Soc.* **1966**, *88*, 380–381.
[6] H. W. Kroto, J. R. Heath, S. C. O'Brien, R. F. Curl, R. E. Smalley, *Nature* **1985**, *318*, 162–163.
[7] S. Iijima, *Nature* **1991**, *354*, 56–58.
[8] S. Kammermeier, P. G. Jones, R. Herges, *Angew. Chem. Int. Ed.* **1996**, *35*, 2669–2671.
[9] M. R. Golder, R. Jasti, *Acc. Chem. Res.* **2015**, *48*, 557–566.
[10] M. A. Majewski, M. Stępień, *Angew. Chem. Int. Ed.* **2019**, *58*, 86–116.
[11] M. Ball, Y. Zhong, Y. Wu, C. Schenck, F. Ng, M. Steigerwald, S. Xiao, C. Nuckolls, *Acc. Chem. Res.* **2015**, *48*, 267–276.
[12] W. Fan, T. Matsuno, Y. Han, X. Wang, Q. Zhou, H. Isobe, J. Wu, *J. Am. Chem. Soc.* **2021**, *143*, 15924–15929.
[13] Q.-H. Guo, Y. Qiu, M.-X. Wang, J. F. Stoddart, *Nat. Chem.* **2021**, *13*, 402–419.
[14] M. Krzeszewski, H. Ito, K. Itami, *J. Am. Chem. Soc.* **2022**, *144*, 862–871.
[15] F. S. Conrad-Burton, T. Liu, F. Geyer, R. Costantini, A. P. Schlaus, M. S. Spencer, J. Wang, R. Hernández Sánchez, B. Zhang, Q. Xu, M. L. Steigerwald, S. Xiao, H. Li, C. P. Nuckolls, X. Zhu, *J. Am. Chem. Soc.* **2019**, *141*, 13143–13147.
[16] C. M. Cruz, J. C. Walsh, M. Juríček, *Org. Mater.* **2022**, *4*, 163–169.
[17] S. Sun, F. S. Conrad-Burton, Y. Liu, F. Ng, M. Steigerwald, X. Zhu, C. Nuckolls, *J. Phys. Chem. A* **2022**, *126*, 7559–7565.
[18] X. Xiao, S. K. Pedersen, D. Aranda, J. Yang, R. A. Wiscons, M. Pittelkow, M. L. Steigerwald, F. Santoro, N. J. Schuster, C. Nuckolls, *J. Am. Chem. Soc.* **2021**, *143*, 983–991.
[19] G. R. Kiel, H. M. Bergman, A. E. Samkian, N. J. Schuster, R. C. Handford, A. J. Rothenberger, R. Gomez-Bombarelli, C. Nuckolls, T. D. Tilley, *J. Am. Chem. Soc.* **2022**, *144*, 23421–23427.
[20] X. Tian, K. Shoyama, B. Mahlmeister, F. Brust, M. Stolte, F. Würthner, *J. Am. Chem. Soc.* **2023**, *145*, 9886–9894.
[21] Y.-Y. Fan, D. Chen, Z.-A. Huang, J. Zhu, C.-H. Tung, L.-Z. Wu, H. Cong, *Nat. Commun.* **2018**, *9*, 3037.
[22] G. Naulet, L. Sturm, A. Robert, P. Dechambenoit, F. Röhricht, R. Herges, H. Bock, F. Durola, *Chem. Sci.* **2018**, *9*, 8930–8936.
[23] K. Senthilkumar, M. Kondratowicz, T. Lis, P. J. Chmielewski, J. Cybińska, J. L. Zafra, J. Casado, T. Vives, J. Crassous, L. Favereau, M. Stępień, *J. Am. Chem. Soc.* **2019**, *141*, 7421–7427.
[24] S. Nishigaki, Y. Shibata, A. Nakajima, H. Okajima, Y. Masumoto, T. Osawa, A. Muranaka, H. Sugiyama, A. Horikawa, H. Uekusa, H. Koshino, M. Uchiyama, A. Sakamoto, K. Tanaka, *J. Am. Chem. Soc.* **2019**, *141*, 14955–14960.
[25] Z. Luo, X. Yang, K. Cai, X. Fu, D. Zhang, Y. Ma, D. Zhao, *Angew. Chem. Int. Ed.* **2020**, *59*, 14854–14860.
[26] Y. Segawa, T. Watanabe, K. Yamanoue, M. Kuwayama, K. Watanabe, J. Pirillo, Y. Hijikata, K. Itami, *Nature Synth.* **2022**, *1*, 535–541.
[27] T. Kawase, H. Kurata, *Chem. Rev.* **2006**, *106*, 5250–5273.
[28] K. Tashiro, T. Aida, *Chem. Soc. Rev.* **2007**, *36*, 189–197.
[29] E. M. Pérez, N. Martín, *Chem. Soc. Rev.* **2008**, *37*, 1512–1519.
[30] C. García-Simón, M. Costas, X. Ribas, *Chem. Soc. Rev.* **2016**, *45*, 40–62.
[31] T. Matsuno, S. Sato, H. Isobe, in *Comprehensive Supramolecular Chemistry II* (Ed.: J. L. Atwood), Elsevier, Oxford **2017**, pp. 311–328.
[32] C. Fuertes-Espinosa, M. Pujals, X. Ribas, *Chem.* **2020**, *6*, 3219–3262.
[33] X. Chang, Y. Xu, M. v. Delius, *Chem. Soc. Rev.* **2024**, *53*, 47–83.
[34] X.-W. Chen, Q.-S. Deng, B.-H. Zheng, J.-F. Xing, H.-R. Pan, X.-J. Zhao, Y.-Z. Tan, *J. Am. Chem. Soc.* **2024**, *146*, 31665–31670.
[35] B. M. White, Y. Zhao, T. E. Kawashima, B. P. Branchaud, M. D. Pluth, R. Jasti, *ACS Cent. Sci.* **2018**, *4*, 1173–1178.
[36] T. C. Lovell, S. G. Bolton, J. P. Kenison, J. Shangguan, C. E. Otteson, F. Civitci, X. Nan, M. D. Pluth, R. Jasti, *ACS Nano* **2021**, *15*, 15285–15293.
[37] S. Xiao, S. J. Kang, Y. Wu, S. Ahn, J. B. Kim, Y.-L. Loo, T. Siegrist, M. L. Steigerwald, H. Li, C. Nuckolls, *Chem. Sci.* **2013**, *4*, 2018–2023.
[38] G. M. Peters, G. Grover, R. L. Maust, C. E. Colwell, H. Bates, W. A. Edgell, R. Jasti, M. Kertesz, J. D. Tovar, *J. Am. Chem. Soc.* **2020**, *142*, 2293–2300.
[39] C. Schaack, A. M. Evans, F. Ng, M. L. Steigerwald, C. Nuckolls, *J. Am. Chem. Soc.* **2022**, *144*, 42–51.
[40] K. Li, S. Yoshida, R. Yakushiji, X. Liu, C. Ge, Z. Xu, Y. Ni, X. Ma, J. Wu, S. Sato, Z. Sun, *Chem. Sci.* **2024**, *15*, 18832–18839.
[41] G. Li, L.-L. Mao, J.-N. Gao, X. Shi, Z.-Y. Huo, J. Yang, W. Zhou, H. Li, H.-B. Yang, C.-H. Tung, L.-Z. Wu, H. Cong, *Angew. Chem. Int. Ed.* **2025**, *64*, e202419435.
[42] Z. Xu, X. Liu, C. Ge, X. Ma, Z. Sun, *Org. Lett.* **2025**, *27*, 7709-7713
[43] T. Kawase, H. R. Darabi, M. Oda, *Angew. Chem. Int. Ed.* **1996**, *35*, 2664–2666.

[44] R. Jasti, J. Bhattacharjee, J. B. Neaton, C. R. Bertozzi, *J. Am. Chem. Soc.* **2008**, *130*, 17646–17647.
[45] H. Takaba, H. Omachi, Y. Yamamoto, J. Bouffard, K. Itami, *Angew. Chem. Int. Ed.* **2009**, *48*, 6112–6116.
[46] S. Yamago, Y. Watanabe, T. Iwamoto, *Angew. Chem. Int. Ed.* **2010**, *49*, 757–759.
[47] N. Kubota, Y. Segawa, K. Itami, *J. Am. Chem. Soc.* **2015**, *137*, 1356–1361.
[48] E. Kayahara, V. K. Patel, A. Mercier, E. P. Kündig, S. Yamago, *Angew. Chem. Int. Ed.* **2016**, *55*, 302–306.
[49] J. M. Van Raden, S. Louie, L. N. Zakharov, R. Jasti, *J. Am. Chem. Soc.* **2017**, *139*, 2936–2939.
[50] P. Della Sala, N. Buccheri, A. Sanzone, M. Sassi, P. Neri, C. Talotta, A. Rocco, V. Pinchetti, L. Beverina, S. Brovelli, C. Gaeta, *Chem. Commun.* **2019**, *55*, 3160–3163.
[51] E. J. Leonhardt, R. Jasti, *Nat. Rev. Chem.* **2019**, *3*, 672–686.
[52] E. R. Darzi, R. Jasti, *Chem. Soc. Rev.* **2015**, *44*, 6401–6410.
[53] S. E. Lewis, *Chem. Soc. Rev.* **2015**, *44*, 2221–2304.
[54] D. Wu, W. Cheng, X. Ban, J. Xia, *Asian J. Org. Chem.* **2018**, *7*, 2161–2181.
[55] D. Lu, Q. Huang, S. Wang, J. Wang, P. Huang, P. Du, *Front. Chem.* **2019**, *7*, 668.
[56] M. Hermann, D. Wassy, B. Esser, *Angew. Chem. Int. Ed.* **2021**, *60*, 15743–15766.
[57] S. Mirzaei, E. Castro, R. Hernández Sánchez, *Chem. - Eur. J.* **2021**, *27*, 8642–8655.
[58] M. Fujitsuka, D. W. Cho, T. Iwamoto, S. Yamago, T. Majima, *Phys. Chem. Chem. Phys.* **2012**, *14*, 14585.
[59] T. Iwamoto, Y. Watanabe, Y. Sakamoto, T. Suzuki, S. Yamago, *J. Am. Chem. Soc.* **2011**, *133*, 8354–8361.
[60] P. Li, T. J. Sisto, E. R. Darzi, R. Jasti, *Org. Lett.* **2014**, *16*, 182–185.
[61] M. Peña-Alvarez, L. Qiu, M. Taravillo, V. G. Baonza, M. C. R. Delgado, S. Yamago, R. Jasti, J. T. L. Navarrete, J. Casado, M. Kertesz, *Phys. Chem. Chem. Phys.* **2016**, *18*, 11683–11692.
[62] M. Fujitsuka, T. Iwamoto, E. Kayahara, S. Yamago, T. Majima, *ChemPhysChem* **2013**, *14*, 1570–1572.
[63] N. Oldani, S. K. Doorn, S. Tretiak, S. Fernandez-Alberti, *Phys. Chem. Chem. Phys.* **2017**, *19*, 30914–30924.
[64] B. N. Taber, C. F. Gervasi, J. M. Mills, D. A. Kislitsyn, E. R. Darzi, W. G. Crowley, R. Jasti, G. V. Nazin, *J. Phys. Chem. Lett.* **2016**, *7*, 3073–3077.
[65] A. P. Alivisatos, *Science* **1996**, *271*, 933–937.
[66] B. Kinkead, T. Hegmann, *J. Mater. Chem.* **2010**, *20*, 448–458.
[67] A. L. Efros, L. E. Brus, *ACS Nano* **2021**, *15*, 6192–6210.
[68] S. Mirzaei, E. Castro, R. Hernández Sánchez, *Chem. Sci.* **2020**, *11*, 8089–8094.
[69] The tolyl group was selected to initially discriminate $\mathbf{p_4}$ and $\mathbf{m_4}$ via MALDI-MS, and subsequently for facile identification of members in the series between the two end points.
[70] J.-N. Gao, A. Bu, Y. Chen, M. Huang, Z. Chen, X. Li, C.-H. Tung, L.-Z. Wu, H. Cong, *Angew. Chem. Int. Ed.* **2024**, *63*, e202408016.
[71] T. C. Lovell, C. E. Colwell, L. N. Zakharov, R. Jasti, *Chem. Sci.* **2019**, *10*, 3786–3790.
[72] F. Bernt, H. A. Wegner, *Chem. - Eur. J.* **2023**, *29*, e202301001.
[73] Deposition Numbers 2405124 (for **1**), 2405125 (for $\mathbf{m_4}$), 2405126 (for $\mathbf{m_3p_1}$), 2405127 (for ***anti*-$\mathbf{m_2p_2}$**), 2422060 (for ***syn*-$\mathbf{m_2p_2}$**) contains the supplementary crystallographic data for this paper. These data are provided free of charge by the joint Cambridge Crystallographic Data Centre and Fachinformationszentrum Karlsruhe Access Structures service.
[74] L. Adamska, I. Nayyar, H. Chen, A. K. Swan, N. Oldani, S. Fernandez-Alberti, M. R. Golder, R. Jasti, S. K. Doorn, S. Tretiak, *Nano Lett.* **2014**, *14*, 6539–6546.
[75] T. J. Sisto, M. R. Golder, E. S. Hirst, R. Jasti, *J. Am. Chem. Soc.* **2011**, *133*, 15800–15802.
[76] J. Xia, R. Jasti, *Angew. Chem. Int. Ed.* **2012**, *51*, 2474–2476.
[77] P. J. Evans, E. R. Darzi, R. Jasti, *Nat. Chem.* **2014**, *6*, 404–408.
[78] E. Kayahara, V. K. Patel, S. Yamago, *J. Am. Chem. Soc.* **2014**, *136*, 2284–2287.
[79] B. M. Wong, *J. Phys. Chem. C* **2009**, *113*, 21921–21927.
[80] T. Nishihara, Y. Segawa, K. Itami, Y. Kanemitsu, *J. Phys. Chem. Lett.* **2012**, *3*, 3125–3128.
[81] T. Nishihara, Y. Segawa, K. Itami, Y. Kanemitsu, *Chem. Sci.* **2014**, *5*, 2293-2296.
[82] J. Kim, R. Kishi, E. Kayahara, W. Kim, S. Yamago, M. Nakano, D. Kim, *Angew. Chem. Int. Ed.* **2020**, *59*, 16989–16996.
[83] S. Chen, X. Miao, H. Zhou, C. Peng, R. Zhang, X. Han, *J. Phys. Chem. A* **2022**, *126*, 7452–7459.
[84] E. Castro, S. Mirzaei, R. Hernández Sánchez, *Org. Lett.* **2021**, *23*, 87–92.
[85] J. Xia, J. W. Bacon, R. Jasti, *Chem. Sci.* **2012**, *3*, 3018.
[86] Y. Segawa, H. Omachi, K. Itami, *Org. Lett.* **2010**, *12*, 2262–2265.
[87] J. Liu, L. Adamska, S. K. Doorn, S. Tretiak, *Phys. Chem. Chem. Phys.* **2015**, *17*, 14613–14622.
[88] B. Rodríguez-Hernández, N. Oldani, A. Martínez-Mesa, L. Uranga-Piña, S. Tretiak, S. Fernandez-Alberti, *Phys. Chem. Chem. Phys.* **2020**, *22*, 15321–15332.
[89] M. Kasha, *Discuss. Faraday Soc.* **1950**, *9*, 14.
[90] X. Zhang, C. Chen, W. Zhang, N. Yin, B. Yuan, G. Zhuang, X.-Y. Wang, P. Du, *Nat. Commun.* **2024**, *15*, 2684.
[91] T. Yanai, D. P. Tew, N. C. Handy, *Chem. Phys. Lett.* **2004**, *393*, 51–57.
[92] All structure names denoted with a prime correspond to DFT-optimized structures with R = Me.
[93] M. Banerjee, R. Shukla, R. Rathore, *J. Am. Chem. Soc.* **2009**, *131*, 1780–1786.
[94] M. Kastler, J. Schmidt, W. Pisula, D. Sebastiani, K. Müllen, *J. Am. Chem. Soc.* **2006**, *128*, 9526–9534.
[95] Q. Zhang, H. Peng, G. Zhang, Q. Lu, J. Chang, Y. Dong, X. Shi, J. Wei, *J. Am. Chem. Soc.* **2014**, *136*, 5057–5064.
[96] J. Zhang, G. Zhou, H.-I. Un, F. Zheng, K. Jastrzembski, M. Wang, Q. Guo, D. Mücke, H. Qi, Y. Lu, Z. Wang, Y. Liang, M. Löffler, U. Kaiser, T. Frauenheim, A. Mateo-Alonso, Z. Huang, H. Sirringhaus, X. Feng, R. Dong, *J. Am. Chem. Soc.* **2023**, *145*, 23630–23638.
[97] D. J. Norris, A. L. Efros, M. Rosen, M. G. Bawendi, *Phys. Rev. B* **1996**, *53*, 16347–16354.
[98] K. E. Knowles, K. H. Hartstein, T. B. Kilburn, A. Marchioro, H. D. Nelson, P. J. Whitham, D. R. Gamelin, *Chem. Rev.* **2016**, *116*, 10820–10851.
[99] Bruker (2015). APEX3. Bruker Analytical X-Ray Systems, Inc.: Madison, Wisconsin, USA.
[100] Bruker (2015). SADABS. Bruker Analytical X-Ray Systems, Inc.: Madison, Wisconsin, USA.
[101] A. Spek, *J. Appl. Cryst.* **2003**, *36*, 7–13.
[102] A. Spek, *Acta Cryst. D* **2009**, *65*, 148–155.
[103] G. M. Sheldrick, *Acta Cryst. A* **2015**, *71*, 3–8.
[104] G. M. Sheldrick, *Acta Cryst. C* **2015**, *71*, 3–8.
[105] O. V. Dolomanov, L. J. Bourhis, R. J. Gildea, J. A. K. Howard, H. Puschmann, *J. Appl. Cryst.* **2009**, *42*, 339–341.
[106] C. G. Jones, M. W. Martynowycz, J. Hattne, T. J. Fulton, B. M. Stoltz, J. A. Rodriguez, H. M. Nelson, T. Gonen, *ACS Cent. Sci.* **2018**, *4*, 1587–1592.
[107] L.-M. Peng, *Acta Cryst. A* **1998**, *54*, 481–485.
[108] A. T. R. Williams, S. A. Winfield, J. N. Miller, *Analyst* **1983**, *108*, 1067-1071.
[109] M. J. Frisch, G. W. Trucks, H. B. Schlegel, G. E. Scuseria, M. A. Robb, J. R. Cheeseman, G. Scalmani, V. Barone, G. A. Petersson, H. Nakatsuji, X. Li, M. Caricato, A. V. Marenich, J. Bloino, B. G. Janesko, R. Gomperts, B. Mennucci, H. P. Hratchian, J. V. Ortiz, A. F. Izmaylov, J. L. Sonnenberg, Williams, F. Ding, F. Lipparini, F. Egidi, J. Goings, B. Peng, A.

Petrone, T. Henderson, D. Ranasinghe, et al., Wallingford, CT, **2016**. https://gaussian.com/citation/
[110] J.-D. Chai, M. Head-Gordon, *Phys. Chem. Chem. Phys.* **2008**, *10*, 6615-6620.
[111] Y. Zhao, D. G. Truhlar, *Theor. Chem. Acc.* **2008**, *120*, 215–241.
[112] H. S. Yu, X. He, S. L. Li, D. G. Truhlar, *Chem. Sci.* **2016**, *7*, 5032–5051.
[113] A. D. Becke, *Phys. Rev. A Gen. Phys.* **1988**, *38*, 3098–3100.
[114] S. Grimme, S. Ehrlich, L. Goerigk, *J. Comput. Chem.* **2011**, *32*, 1456–1465.
[115] E. Cancès, B. Mennucci, J. Tomasi, *J. Chem. Phys.* **1997**, *107*, 3032–3041.
[116] T. Lu, F. Chen, *J. Comput. Chem.* **2012**, *33*, 580–592.
[117] Z. Liu, T. Lu, Q. Chen, *Carbon* **2020**, *165*, 461–467.
[118] T. Lu, *J. Chem. Phys.* **2024**, *161*, 082503.
[119] N. M. O'Boyle, A. L. Tenderholt, K. M. Langner, *J. Comput. Chem.* **2008**, *29*, 839–845.

Manuscript received: May 20, 2025
Revised manuscript received: July 21, 2025
Accepted manuscript online: July 22, 2025
Version of record online: ■■, ■■